Influence of enhanced Asian NO$_x$ emissions on ozone in the Upper Troposphere and Lower Stratosphere (UTLS) in chemistry climate model simulations

Chaitri R.[1], Suvarna Fadnavis[1*], Rolf Müller[2], Ayantika D. C.[1], Felix Ploeger[2], Alexandru Rap[3]

[1]Indian Institute of Tropical Meteorology, Pune, India

[2]Forschungszentrum Jülich GmbH, IEK7, Jülich, Germany

[3]School of Earth and Environment, University of Leeds, Leeds, United Kingdom

*Email of corresponding author: suvarna@tropmet.res.in

Abstract:

The Asian summer monsoon (ASM) anticyclone is the most pronounced circulation pattern in the Upper Troposphere and Lower Stratosphere (UTLS) during the Northern Hemisphere summer. Asian summer monsoon convection plays an important role in efficient vertical transport from the surface to the upper-level anticyclone. In this paper we investigate the potential impact of enhanced anthropogenic nitrogen oxides (NO$_x$) emissions on the distribution of ozone in the UTLS using the fully-coupled aerosol chemistry climate model, ECHAM5-HAMMOZ. Ozone in the UTLS is influenced both by the convective uplift of ozone precursors and by the uplift of enhanced NO$_x$ induced tropospheric ozone anomalies. We performed anthropogenic NO$_x$ emission sensitivity experiments over India and China. In these simulations, covering the years 2000-2010 anthropogenic NO$_x$ emissions have been increased by 38% over India and by 73% over China with respect to the emission base year 2000. These emission increases are comparable to the observed linear trends of 3.8 % per year over India and 7.3% per year over China during the period 2000 to 2010. Enhanced NO$_x$ emissions over India by 38 % and China by 73 % increase the ozone radiative forcing in the ASM Anticyclone (15°-40°N, 60°-120°E) by 16.3 mW m^{-2} and 78.5 mW m^{-2} respectively. These elevated NO$_x$ emissions produce significant warming over the Tibetan Plateau and increase precipitation over India due to a

25 strengthening of the monsoon Hadley circulation. However increase in NO_x emissions over India by

26 73% (similar to the observed increase over China), results in large amount of ozone production over the

27 Indo Gangetic plain and Tibetan Plateau. The higher ozone concentrations, in turn, induce a reversed

28 monsoon Hadley circulation and negative precipitation anomalies over India. The associated

29 subsidence suppresses vertical transport of NO_x and ozone into the ASM anticyclone.

30 Key words: Asian summer monsoon, Tropospheric ozone, Tropospheric NO_x, NO_x transport, Upper

31 troposphere and lower stratosphere, Ozone radiative forcing.

32

33 **1. Introduction**

34 Rapid economic development and urbanization in Asia has resulted in an unprecedented growth in

35 anthropogenic emissions of nitrogen oxides (NO_x), carbon monoxide (CO), carbon dioxide (CO_2),

36 methane (CH_4). Many of these species affect concentrations of tropospheric ozone, which is both an

37 important polluting agent and a greenhouse gas (Wild and Akimoto, 2001; Chatani et al 2014; Revell et

38 al., 2015). Ground based and satellite observations show a large amount of these ozone precursors

39 concentrated over India and China (Sinha et al., 2014; Richter et al., 2005; Jacob et al., 1999; Zhao et

40 al., 2013; Gu et al., 2014). Studies show that tropospheric ozone production over Asia is controlled by

41 the abundance of NO_x and VOCs (Sillman, 1995, Lei et al., 2004, Zhang et al., 2004 and Tie et al.,

42 2007), with large regions such as India and China being NO_x limited regions. Therefore, increased NO_x

43 in these regions leads to an increase in ozone concentrations (Yamaji et al., 2006; Sinha et al., 2014;

44 Fadnavis et al., 2014). Recently, positive trends in Asian tropospheric column NO_2 have been reported,

45 i.e. 3.8 % yr^{-1} over India, using SCanning Imaging Absorption SpectroMeter for Atmospheric

46 CHartographY (SCIAMACHY) observations for the period 2003-2011 (Ghude et al., 2013), and 7.3%

47 yr^{-1} over China using Ozone Monitoring Instrument (OMI) observations for the period 2002-2011

48 (Schneider and van der A., 2012). Lightning contributes to the production of NOx in the middle and

upper troposphere (Barret et al, 2016). Over the Asian region, lightning contributes ~40% to NO_x and 20% to ozone production in the middle and upper troposphere during the monsoon season (Tie et al. 2001; Fadnavis et al. 2015). The upper tropospheric ozone concentration is determined by in-situ production from both lightning and ozone precursors which are transported from the boundary layer (Sὅvde et al., 2011; Barret et al, 2016).

Tropospheric ozone has a warming effect on climate, its estimated radiative forcing due to increased concentrations since pre-industrial times being $0.4 \, \mathrm{W \, m^{-2}}$, with a 5 to 95% confidence range of $(0.2 \, \mathrm{to} \, 0.6 \, \mathrm{W \, m^{-2}})$ (Stevenson et al., 2013; Myhre et al., 2013). Previous studies highlighted the importance of the tropical tropopause region for ozone radiative forcing (Lacis et al, 1990; Riese et al., 2012; Rap et al., 2015) and showed that ozone perturbations exert a large influence on the thermal structure of the atmosphere (e.g., Thuburn and Craig, 2002; Foster and Shine 1997). A recent study based on Atmospheric Chemistry and Climate Model Intercomparison Project (ACCMIP) models reported that NO_x and CH_4 are the greatest contributors in determining tropospheric ozone radiative forcing (Stevenson et al., 2013).

Asian Summer Monsoon (ASM) convection efficiently transports Asian pollutants from the boundary layer into the Upper Troposphere and Lower Stratosphere (UTLS) (Randel and Park, 2006; Randel et al. 2010; Fadnavis et al., 2013, 2015). Studies pertaining to modeling and trajectory analysis confirm this finding (Li et al., 2005; Park et al., 2007; Randel et al., 2010; Chen et al., 2012; Vogel et al., 2015, 2016). Satellite observations show the confinement of a number of chemical constituents like water vapor (H_2O), CO, CH_4, ethane, hydrogen cyanide (HCN), PAN and aerosols, within the ASM anticyclone (Park et al., 2004, 2007, 2008; Li et al., 2005; Randel and Park, 2006; Xiong et al., 2009; Randel et al. 2010; Lawrence et al., 2011; Abad et al., 2011; Fadnavis et al., 2013;2014;2015; Barret et al., 2016) which has potential implications on stratospheric chemistry and dynamics. Thus the rise in anthropogenic emissions over the ASM region alters the chemical composition of the UTLS (Lawrence

73 et al., 2011; Fadnavis et al, 2014, 2015) during the monsoon season. Another prominent feature of the

74 satellite observations is an ozone minimum in the ASM anticyclone (near 100 hPa) (Gettelman et al.,

75 2004; Konopka et al., 2010; Braesicke et al., 2011). This ozone minimum is linked to upward transport

76 of ozone poor air masses (Gettelman et al., 2004; Park et al., 2007; Kunze et al., 2010). Observations

77 show that convectively lifted air masses arriving in the anticyclone are ozone poor but rich in ozone

78 precursors. Balloon sonde observations show that ozone variations near the anticyclone are strongly

79 correlated with temperature near the tropopause (Tobo et al., 2008). Thus the linkage of low ozone and

80 high concentrations of ozone precursors with the temperature variation in the anticyclone is an open

81 question.

82   In this study we ask the question 'how do increasing Asian NO_X emissions and the associated

83 ozone production affect ozone radiative forcing and monsoon circulation?'. We perform sensitivity

84 experiments of increased anthropogenic NO_x emissions using the state-of-the-art ECHAM5-HAMMOZ

85 (European Centre General Circulation Model version5) chemistry climate model (Roeckner et al.,

86 2003; Horowitz et al., 2003; Stier et al., 2005). We estimate the ozone radiative forcing for the different

87 anthropogenic NO_x emission scenarios, together with associated changes in temperature and the

88 monsoon circulation. The paper is organized as follows: in Section 2 the data and model set up are

89 described; the results are summarized in Section 3 and discussed in Section 4, followed by conclusions

90 given in Section 5.

91

92 **2. Data description and Model setup**

93 **2.1 Satellite measurements**

94   Earth Observing System (EOS) microwave limb sounder (MLS) is one of the four instruments

95 on the NASA's EOS Aura satellite flying in the polar sun-synchronous orbit. It measures the thermal

96 emissions at millimeter and sub millimeter wavelengths (Waters et al., 2006). It performs 240 limb

97   scans per orbit with a footprint of ∼6 km across-track and ∼200 km along-track, providing ∼3500

98   profiles per day. MLS also measures vertical profiles of temperature, ozone, CO, H_2O, and many other

99   constituents in the mesosphere, stratosphere and upper troposphere (Waters et al., 2006). In the UTLS,

100 MLS has a vertical resolution of about 3 km. MLS vertical profiles of ozone show good agreements

101 with the Stratospheric Aerosol and Gas Experiment II (SAGE-II), Halogen Occultation Experiment

102 (HALOE), Atmospheric Chemistry Experiment (ACE) and ozonesonde measurements (Froidevaux et

103 al.,2006). The MLS ozone profiles are considered to be useful in the range of 215 − 0.46 hPa (Livesey

104 et al., 2005). In this study we analyze the MLS level 2 (version 4) ozone mixing ratios data for the

105 period 2004 − 2013. The data has been gridded horizontally, within latitude bins of equal area (with the

106 equatorial bin of 150km width) and longitude bins of about 8.5 degrees. This data can be accessed from

107 http://mls.jpl.nasa.gov/. For comparison, simulated ozone is convolved with the MLS averaging kernel

108 (Livesey et al. 2011).

109

110 **2.2 Model simulation and experimental setup**

111   We employ the aerosol-chemistry-climate model ECHAM5-HAMMOZ which comprises the

112 general circulation model ECHAM5 (Roeckner et al., 2003), the tropospheric chemistry module,

113 MOZART2 (Horowitz et al 2003) and the aerosol module, Hamburg aerosol model (HAM) (Stier et al.,

114 2005). It includes NO_x, VOC and aerosol chemistry. The gas phase chemistry is based on the chemical

115 scheme provided by the MOZART-2 model (Horowitz et al., 2003) which includes detailed chemistry

116 of the O_x-NO_x hydrocarbon system with 63 tracers and 168 reactions. The O(^{1}D) quenching reaction

117 rates used are taken from Sander et al., (2003) and isoprene nitrates chemistry taken from Fiore et al.,

118 (2005). The dry deposition in ECHAM5-HAMMOZ follows the scheme given by Ganzeveld and

119 Lelieveld (1995). Soluble trace gases like HNO_3 and SO_2 are also subject to wet deposition. In-cloud

120 and below-cloud scavenging follows the scheme given by Stier et al. (2005). Interactive calculation of

cloud droplet number concentration is according to Lohmann et al (1999) and ice crystal number concentrations are according to Kärcher and Lohmann (2002). The convection scheme is based on the mass flux scheme developed by Tiedke (1989). Lightning NO_x emissions are parameterized following Grewe et al. (2001).

The model is run at a T42 spectral resolution corresponding to about 2.8°×2.8° in the horizontal dimension and 31 vertical hybrid $\sigma - p$ levels from the surface to 10 hPa. In our model simulations, emissions from anthropogenic sources and biomass burning are from the year 2000 RETRO project data set (available at http://eccad.sedoo.fr/) (Schultz et al., 2004; 2005; 2007; 2008). Emissions of SO_2, BC and OC are based on the AEROCOM-II emission inventory, also for the year 2000 (Dentener et al., 2006). The distribution of NO_x emission mass flux (kg m^{-2} s^{-1}) averaged for the Asian summer monsoon season (June–September) is shown in Supplementary Fig. S1. It shows high values over the Indo Gangetic Plains and East China. Other details of model parameterizations, emissions and evaluation are described by Fadnavis et al. (2013; 2014; 2015) and Pozzoli et al. (2008a, b; 2011). Each of our model experiments consists of continuous simulations for eleven years from 2000 to 2010. The base year for emissions is taken as 2000 and emissions were repeated every year throughout the simulation period. Meteorology varied due to varying monthly mean sea surface temperature (SST) and sea ice concentration (SIC). The AMIP2 SSTs and SIC varying for the period 2000 − 2010 were specified as a lower boundary condition.

In order to understand the impact of enhanced anthropogenic NO_x emissions on the distribution of ozone in the UTLS, sensitivity simulations were performed for the period 2000 − 2010. The experimental set up is the same as described by Fadnavis et al. (2015). The four simulations analyzed in this study are: (1) a reference experiment (CTRL) and three sensitivity experiments (referred to as experiments 2 - 4), where the anthropogenic NO_x emissions over India and China are scaled in accordance with the observed trends. In experiment (2), anthropogenic NO_x emissions are increased

145   over India by 38% (Ind38), in experiment (3) increases over China by 73% (Chin73) are prescribed. In

146   order to analyze the effects of similar NO_x percentage increases over India and China, NO_x emissions

147   are increased over India by 73% (Ind73) in experiment (4). The emission perturbations were obtained

148   from observed NO_2 trends of 3.8% per year over India (Ghude et al., 2013) and 7.3% per year over

149   China (Schneider and van der A., 2012). Hiboll et al. (2013) also reported similar increasing NO_x

150   values over megacities in India and China. All four simulations use the same VOC and CO emissions

151   and they all include NO_x production due to lightning (lightning-on) and soil emissions. There may be

152   indirect impact of lightning NO_x emission. Since it is same in CTRL and sensitivity simulations its

153   impact may be negligible.

154   In addition, a lightning-off simulation was performed for the same period and boundary

155   conditions as experiments 1-4 (this simulation is the same as the one described in Fadnavis et al.

156   (2015)). The impact of lightning on NO_x production is estimated by comparing the CTRL (lightning-

157   on) with lightning-off simulations.

158   The accuracy of the simulation of the monsoon circulation probably depends on model

159   resolution and an increased vertical resolution may improve the model performance (Druyan et al.,

160   2008; Abhik et al., 2014). However, the model resolution of T42L31 is capable of reasonably

161   simulating the general regional spatial pattern of precipitation and low-level circulation (Rajeevan et

162   al., 2005) (see Supplementary Fig. S2, showing simulated seasonal mean precipitation and circulation

163   at 850 hPa in the CTRL simulation).

164   The heating rates and radiative forcings associated with the ozone changes in our three

165   sensitivity simulations are calculated using the Edwards and Slingo (1996) radiative transfer model and

166   the fixed dynamical heating approximation for stratospheric temperature adjustment. Similarly to

167   previous studies (Riese et al., 2012; Bekki et al., 2013; Rap et al., 2015), we used the off-line version of

168   the model, with six shortwave and nine longwave bands, and a delta-Eddington 2-stream scattering

7

169 solver at all wavelengths.

170

3. Results

3.1 Comparison with MLS satellite measurements in the UTLS

173   The spatial distributions of ozone mixing ratios from MLS observations at 100 hPa and from

174 the CTRL ECHAM5-HAMMOZ simulation at 90 hPa (the nearest model level) after smoothing with

175 the averaging kernel of MLS are illustrated in Fig. 1a and Fig. 1b, respectively. For comparison we

176 have interpolated the model data to the MLS pressure grid, then applied the MLS averaging kernel and

177 finally interpolated back to the model pressure grid. The climatological horizontal winds plotted in the

178 figure clearly show the anticyclonic upper level monsoon circulation. Recent attempts to characterize

179 the extent of the anticyclone are based either on potential vorticity on isentropic surfaces or

180 geopotential height on pressure surfaces. Here we apply both characterizations of the anticyclone and

181 show the PV contour related to the maximum PV gradient on 380K (calculated from ERA-Interim

182 reanalysis following Ploeger et al., 2015), and the 270m geopotential height anomaly as proposed by

183 Barret et al. (2016). The close agreement of both methods shows that from a climatological point of

184 view the two criteria yield a very similar picture of the anticyclonic circulation and the related trace gas

185 confinement. Locally and at particular dates, however, differences may be larger with potential

186 vorticity correlating better with confined trace gas anomalies than geopotential height (e.g., Garny and

187 Randel, 2013; Ploeger et al., 2015). The spatial pattern of low ozone concentrations in the monsoon

188 anticyclone is well simulated in the model. It is in good agreement with MLS (90-140 ppbv), MIPAS

189 (80-120 ppbv) and SAGE II (<150ppbv) measurements (Kunze et al., 2010; Randel et al., 2001; Randel

190 and Park 2006; Park et al., 2007).

191   Vertical profiles of ozonesonde measurements (averaged for the monsoon season during 2001-

192 2009) at Indian stations, Delhi (28.61ºN, 77.23ºE), Pune (18.52ºN, 73.85ºE) and Thiruvananthapuram

193 (8.48ºN, 76.95E) are compared with MLS measurements and ECHAM5-HAMMOZ simulated ozone

194 mixing ratios in Figs. 1(c)-(e). ECHAM5-HAMMOZ simulations show good agreement with MLS data

195 between 200 hPa and 50 hPa at all three stations. Comparison of ozonesonde observations with the

196 ECHAM5-HAMMOZ simulation shows reasonably good agreement at Pune, compared to Delhi and

197 Thiruvananthapuram where there are some discrepancies. The simulated ozone mixing ratios are lower

198 than ozonesonde measurements by 10-40 ppb between 500 – 90 hPa at Pune and by ~70-90 ppb in the

199 upper troposphere (500-150 hPa) at Delhi. At Thiruvananthapuram, while at altitudes below 375 hPa,

200 simulated ozone mixing ratios show good agreement with ozonesonde data, at the altitudes above 375

201 hPa, simulated values are lower than observations by ~20-70 ppb. The differences between model and

202 ozonesonde data may be due to different grid sizes: the ECHAM5-HAMMOZ model grid size is ~280

203 km, while balloon observations are within ~30-180 km spatial range (balloon typically drifts ~30–180

204 km horizontally). In addition, previous work comparing these model simulations with various aircraft

205 observations during the monsoon season, found a reasonable agreement for PAN, NO_x, HNO_3 and O_3

206 mixing ratios (Fadnavis et al., 2015).

207

208 **3.2 Transport of enhanced NO_x emissions into the UTLS**

209 Recent satellite observations and model simulations demonstrated the impact of convective

210 transport of boundary layer pollution into the ASM anticyclone during the Asian summer monsoon

211 season (Gettelman et al., 2004; Randel et al., 2010; Fadnavis et al., 2013, 2014, 2015). These pollutants

212 are further transported across the tropopause as evident in satellite observations of, e.g. water vapour

213 (Bian, 2012), hydrogen cyanide (HCN) (Randel, 2010), CO (Schoeberl et al., 2006), Peroxyacetyl

214 nitrate (PAN) (Fadnavis et al.,2014; 2015), aerosols (Vernier et al., 2015, Fadnavis et al., 2013). To

215 understand the influence of monsoon convection on the vertical distribution of NO_x we show zonal and

216 meridional cross sections over India and China. Vertical distributions of NO_x averaged for the monsoon

season over Indian latitudes (8°N-35°N), and Chinese latitudes (20°N-45°N) as obtained from CTRL simulations are shown in the Supplementary Figs. S3(a) and S3(b) respectively. These figures show elevated levels of NO_x extending from the surface to the upper troposphere over India and China. The wind vectors along with the distribution of cloud droplet number concentration (CDNC) and ice crystal number concentration (ICNC), (Supplementary Figs. S4(a), S4(b) and S4(c)) indicate strong convective transport from the Bay of Bengal (BOB), South China Sea and southern slopes of Himalayas which might lift the boundary layer NO_x to the upper troposphere.

During the monsoon season, the NO_x distribution in the UTLS is also influenced by lightning, in addition to transport from anthropogenic sources. Lightning activity during this season was found to be more pronounced in Asia, compared to the other monsoon regions such as North America, South America and Africa (Ranalkar and Chaudhari, 2009; Penki and Kamra, 2013). In our simulations, we find that lightning produces 40-70% of NO_x over north India and Bay of Bengal and 40-60% over the Tibetan Plateau and West China region (Supplementary Fig. S5).

Fig. 2 shows the vertical distribution of anthropogenic NO_x anomalies obtained from the Ind38, Ind73, Chin73 simulations, compared with the CTRL simulation. Ind38 simulation shows that the convective winds over the Bay of Bengal (80-90°E) (Fig. 2(a)) and at the southern flank of the Himalayas (Fig. 2(d)) lift up the enhanced Indian NO_x emissions to the upper troposphere (UT). Similarly the Chin73 simulation shows that the convective winds over the South China Sea (100-120°E) (Fig. 2(c)) and over the Himalayas (Fig. 2(f)) lift up the enhanced Chinese NO_x emissions to the UT. While most transport is mainly into the UT, parts of it also occur into the lower stratosphere, with cross tropopause transport being particularly evident in the Chin73 simulation (Figs. 2(c) and 2(f)). Randel and Park (2006) and Randel et al. (2010) also reported that pollution transported by Asian monsoon convection enters the stratosphere. Our results are also in good agreement with previous studies indicating significant vertical transport due to strong monsoon convection from the southern

241 slopes of Himalayas (Fu et al., 2006, Fadnavis et al., 2013; 2014) and the South China Sea (Park et al

242 2009; Chen et al., 2012). In the upper troposphere, NO_x is transported over Iran and Saudi Arabia along

243 the descending branch of the large scale monsoon circulation (Rodwell and Hoskins, 1995). However,

244 the cross tropopause transport is not present in the Ind73 simulation, where it is inhibited by the wind

245 anomalies that show a descending branch over central India (~20°N, 75°E) (Figs. 2(b) and 2(e)). These

246 descending wind anomalies may also be related to the associated ozone radiative forcing and

247 temperature changes, as discussed in Section 4.

248

249 **3.3 Impact of enhanced anthropogenic NO_x on the tropospheric ozone distribution**

250   We calculate the change in ozone production over India and China due to enhanced NO_x

251 emissions in the Ind38, Ind73 and Chin73 simulations with respect to the CTRL simulation. Figure 3,

252 showing longitude-pressure cross sections of net ozone production (ppt/day) changes, indicates that the

253 majority of this additional ozone production occurs in the lower troposphere. At altitudes below 300

254 hPa, the ozone production and loss vary between -15 ppt day^{-1} and 15 ppt day^{-1}. In the upper

255 troposphere (300-150 hPa), the estimated amount of additional net ozone production in Ind38 and

256 Ind73 simulation is 3-7 ppt day^{-1}, while in the Chin73 simulation it is ~3-13 ppt day^{-1}. We also simulate

257 ozone loss near the tropopause in the Ind73 simulation (Fig. 3(b)). We note that these ozone anomalies

258 are not driven by lightning NO_x, as this is included in all simulations. It is interesting to understand

259 ozone production over the highly populated Indo Gangetic Plain and Tibetan Plateau region (these

260 regions are marked in Fig. S4). A longitude pressure cross section over this region show that ozone

261 production over the Indo Gangetic Plain and Tibetan Plateau in Ind73 is (20-25ppt day^{-1}) is much larger

262 than Ind38 (6-20 ppt day^{-1}) in the lower troposphere (Supplementary Fig. S6).

263   Figure 4 shows the vertical distribution of ozone anomalies induced by enhanced anthropogenic

264 NO_x emissions in the three perturbation experiments compared to the CTRL simulation, averaged over

265   India and China. Although the air mass in the monsoon anticyclone is relatively poor in ozone

266   (Fig.1(b)), the elevated amounts of ozone anomalies in response to enhanced anthropogenic NO_x

267   emissions are clearly seen in Fig. 4. This may be partially due to convective transport of enhanced-

268   NO_x-emission induced ozone anomalies produced in the lower troposphere, and partially due to

269   chemical ozone production from convectively transported boundary layer ozone precursors. Ozone

270   anomalies are enhanced near 300-200 hPa over west Asia (40-60ºE) (Figs. 4a-c), possibly due to the

271   vertical convective transport of ozone anomalies and precursors and also from subsequent horizontal

272   transport in the monsoon anticyclone (Barret et al., 2016).

273   Latitude-pressure cross sections of enhanced NO_x emission induced ozone anomalies plotted in

274   Figs. 4(d) and 4(f) illustrate how convection over the Bay of Bengal, the southern slopes of the

275   Himalayas and the South China Sea lifts the enhanced ozone anomalies from India and China into the

276   upper troposphere. These ozone anomalies are also transported further across the tropopause and into

277   the lower stratosphere, where ozone production is also driven by photolysis and NO_x anomalies.

278   In the Ind73 simulation, similarly to the NO_x anomaly distribution (Figs. 2(b) and 2(e)), the

279   descending branch of circulation over central India also suppresses the vertical transport of ozone

280   anomalies across the tropopause (Figs. 4(b) and 4(e)). This subsidence may be related to ozone heating

281   rate changes, as there is significant increase in ozone production over the Indo Gangetic plain and

282   Tibetan Plateau in the lower troposphere due to enhanced anthropogenic NO_x emissions (Section 4).

283

284   **3.4 Distribution of NO_x and ozone in the anticyclone**

285   The distributions of NO_x and ozone anomalies in the monsoon anticyclone region in the Ind38,

286   Ind73 and Chin73 simulations with respect to the CTRL simulation are shown in Figs. 5(a)-(f). A

287   maximum in the NO_x anomalies in the ASM anticyclone (60°E to 120°E) is seen in all the simulations.

288   NO_x anomalies are high at the eastern part of the monsoon anticyclone since convective injection into

289   the anticyclone occurs mainly in that region (Fadnavis et al., 2013). Increase in NO_x anomalies in the

290   Ind38 simulation is higher (Fig. 5(a)) than that in the Ind73 simulation (Figs. 5(b)), mainly due to

291   descending motion over central India in the Ind73 simulation, as seen in the previous sections. In

292   contrast to NO_x anomalies, ozone anomalies in Ind38 are lower than Ind73, especially in the north-

293   eastern part of anticyclone. Satellite observations also show high ozone precursors and low ozone

294   amounts in the anticyclone (Park et al., 2007; Barret et al., 2016). Similarly, the Chin73 simulation

295   shows higher values of NO_x anomalies (>18%) and strong negative ozone anomalies (~-8%) in the

296   north eastern region of the monsoon anticyclone (Figs. 5(c) and 5(f)). Figure 5 also shows that the

297   tropical easterly jet transports NO_x and ozone (from India and China) to Saudi Arabia, Iran and Iraq.

298

299   **4. Discussion**

300   To estimate the radiative impact of the simulated ozone changes, we use the offline version of

301   the Edwards and Slingo (1996) radiative transfer model. Figure 6 shows the radiative forcing caused by

302   the ozone changes in each of the three sensitivity simulations compared to the CTRL simulation. The

303   overall increase in tropospheric ozone (see Figure 4) has a warming effect on climate, with the regional

304   average radiative forcing in the monsoon anticyclone (15ºN-40ºN, 60-120ºE) estimated at16.3 mW m^{-2},

305   69.9 mW m^{-2}, and 78.5 mW m^{-2} in the Ind38, Ind73, and Chin73 simulations, respectively.

306   We also investigate the impact on the atmospheric heating rates caused by the ozone changes.

307   Figure 7 shows the zonal mean heating rate anomalies for the Ind38, Ind73 and Chin73 simulations,

308   compared to the CTRL simulation. These three simulations show positive and negative heating rates

309   anomalies between 400-200 hPa. However, in the upper troposphere and lower stratosphere (200-50

310   hPa) ozone heating rates are negative over Indo Gangetic plain (20-30°N) and Tibetan Plateau (30-

311   40ºN) region. In Ind73 simulation, ozone heating rate anomalies are positive in the lower troposphere

312   over the Indo Gangetic plain (1000-750 hPa) and Tibetan plateau (600-400 hPa). This may be due to

13

313   large amount of ozone production in the lower troposphere over these regions (Fig. S6). This heating

314   may produce changes in the circulation leading to ascending motion over the Tibetan Plateau and a

315   descending branch over central India (~20ºN), i.e. a reversal of monsoon Hadley circulation (Fig. 9(b)).

316   Figures 8 shows latitude pressure cross-section of temperature anomalies (K) obtained from

317   Ind38, Ind73 and Chin73 simulations. Ind38 and Chin73 simulations show anomalous warming in the

318   upper troposphere over the Tibetan Plateau while it is subdued in the Ind73 simulation. Upper

319   tropospheric warming over the Tibetan plateau is one of the key factors responsible for the ASM

320   circulation (Flohn 1957; Yanai et al., 1992; Meehl, 1994; Li and Yanai, 1996; Wu and Zhang, 1998).

321   Flohn (1957, 1960) suggested that upper tropospheric warming over the Tibetan plateau leads to

322   increased Indian summer monsoon rainfall by enhancing the cross-equatorial circulation that brings

323   rainfall to India (Rajagopalan and Molnar, 2013, Vinoj et al., 2014). Goswami et al., (1999) also

324   reported that there is a strong correlation between Hadley circulation and monsoon precipitation.

325   Figures 9(a)-(c) depict the change in monsoon Hadley cell circulation (averaged over 70ºE-

326   100ºE) obtained from the difference in the Ind38, Ind73 and Chin73 and CTRL simulations. The Ind38

327   and Chin 73 simulations show a strengthening of the Hadley circulation; a strong ascending branch of

328   the Hadley cell around 10º-20ºN (Fig. 9(a)), whereas the tilted descending branch of Hadley cell is seen

329   over 20ºN in the Ind73 simulation (Fig. 9(b)). In Ind73 simulation ozone heating rates are positive and

330   negative in the vertical direction near ~20ºN (Fig 7 (b)) which might have attributed tilted descending

331   branch of Hadley cell. Consequently, precipitation anomalies over the Indian region (70º-90º E; 8º-35º

332   N) are positive (0.3 to 0.9 mm day^{-1}) in the Ind38 and Chin73 simulations (Figs. 9(d) and 9(f)), whereas

333   they are negative in the Ind73 simulation (-0.3 to -0.6 mm day^{-1}) (Fig. 9(e)). In the upper troposphere

334   (250 hPa-100 hPa), Ind73 simulation shows subsidence while Chin73 simulation shows ascending

335   motion at these levels over the Indian region. Upper tropospheric subsidence in Ind73 simulation might

336   have contributed to the weak positive and negative precipitation anomalies over the North Indian

14

337   region (Fig. 9(e)). The Chin73 simulation shows subsidence near 22°N below 200 hPa and ascending

338   motion above it. The Chin73 simulation shows ascending motion near 12ºN rising up to 110 hPa, which

339   leads to positive precipitation anomalies over the Indian peninsula.

340   Thus, enhanced Indian (Ind38) and Chinese (Chin73) NO_x emissions increase warming over the

341   Tibetan plateau and enhance precipitation over India via a strengthening of the monsoon Hadley

342   circulation. Remarkably, a further increase of NO_x emissions over India (Ind73) leads to high amounts

343   of ozone in the lower troposphere over the Indo Gangetic plain and Tibetan Plateau. The related ozone

344   heating induces a reversal of the monsoon Hadley circulation, thereby resulting in negative

345   precipitation anomalies.

5. Conclusions

347   In this paper we investigate the potential impacts of enhanced anthropogenic NO_x emissions on

348   ozone production and distribution during the monsoon season using the state-of-the-art ECHAM5-

349   HAMMOZ model simulations. We performed sensitivity experiments for anthropogenic NO_x

350   enhancements of 38% over India (Ind38 simulation) and 73% over China (Chin73 simulation) in

351   accordance with recently observed trends of 3.8% per year over India and 7.3% per year over China

352   (Ghude et al., 2013; Schneider and van der A., 2012). In another experiment, anthropogenic NO_x

353   emissions over India are increased by 73%, equal to Chinese emissions (Ind73 simulation).

354   These simulations show that an increase in anthropogenic NO_x emissions (over India and

355   China) increases ozone production in the lower and mid-troposphere. The monsoon convection at the

356   southern flank of the Himalayas (80-90°E) and over the Bay of Bengal lifts up the NO_x and ozone

357   anomalies from India across the tropopause into the lower stratosphere (Fig. 2(a)-(c), Fig. 4(a)-(b) and

358   Fig. S4). Cross tropopause transport also occurs over China due to convection over the South China

359   Sea.

15

360   Increase in NO_x emissions in the Ind38, Ind73 and Chin73 simulations leads to increase in

361   ozone radiative forcings, in the anticyclone (15ºN-40ºN, 60ºE-120ºE) of 16.25 mWm^{-2}, 69.88 mW m^{-2},

362   and 78.51 mW m^{-2} in the Ind38, Ind73, and Chin73 simulations, respectively. Enhanced ozone

363   production (Ind38 and Chin73 simulations) increases ozone heating rates which cause anomalous

364   warming over the Tibetan plateau. Further increase in NO_x emissions over the India region (Ind73

365   simulation) produces anomalous heating in the lower troposphere over the Indo Gangetic Plain and

366   Tibetan Plateau. This warming elicits the reversal of the monsoon Hadley cell circulation. The

367   descending branch of the monsoon Hadley circulation over the central India impedes vertical transport

368   of ozone and NO_x anomalies.

369   In the Ind38 and Chin73 simulations, anomalous warming over the Tibetan plateau results in a

370   strengthening of the monsoon Hadley circulation over India and elicits positive precipitation (0.3 to 0.9

371   mm day^{-1}) anomalies over India. However, in Ind73 simulations the reversal of the Hadley circulation

372   and the concurrent subdued warming in the upper troposphere over the Tibetan plateau results in

373   negative precipitation anomalies (-0.3 to -0.6 mm day^{-1}) over India.

374

383

References:

Abad G. G., Allen N. D. C., Bernath P. F., Boone C. D., McLeod S. D., Manney G. L., Toon G. C., Carouge C., Wang Y., Wu S., Barkley M. P., Palmer P. I., Xiao Y., and Fu T. M.: Ethane, ethyne and carbon monoxide concentrations in the upper troposphere and lower stratosphere from ACE and GEOS-Chem: a comparison study, Atmos. Chem. Phys., 11, 9927–9941, 2011. doi:10.5194/acp-11-9927-2011, 2011.

Abhik S., Mukhopadhyay P., Goswami B. N., Evaluation of mean and intraseasonal variability of Indian summer monsoon simulation in ECHAM5: identification of possible source of bias, Climate Dynamics, Volume 43, Issue 1, pp 389–406, 2014.

Barret, B., Sauvage, B., Bennouna, Y., and Le Flochmoen, E.: Upper-tropospheric CO and O_3 budget during the Asian summer monsoon, Atmos. Chem. Phys., 16, 9129-9147, doi:10.5194/acp-16-9129-2016, 2016.

Bekki, S., Rap, A., Poulain, V., Dhomse, S., Marchand, M., Lefevre, F., Forster, P. M., Szopa, S. and Chipperfield, M. P.: Climate impact of stratospheric ozone recovery, Geophys. Res. Lett., 40(11),2796-2800,doi:10.1002/grl.50358,2013.

Bian, J., Pan, L. L., Paulik, L., Vömel, H., Chen, H., and Lu, D.: In situ water vapor and ozone measure-ments in Lhasa and Kunming during the Asian summer monsoon, Geophys. Res. Lett., 39, L19808, doi:10.1029/2012GL052996, 2012.

Braesicke, P., Smith, O. J., Telford, P., & Pyle, J. A.: Ozone concentration changes in the Asian summer monsoon anticyclone and lower stratospheric water vapour: An idealised model study. Geophysical Research Letters, 38(3), doi: 10.1029/2010GL046228, 2011.

Chatani, S., Amann, M., Goel, A., Hao, J., Klimont, Z., Kumar, A., Mishra, A., Sharma, S., Wang, S. X., Wang, Y. X., and Zhao, B.: Photochemical roles of rapid economic growth and potential abatement strategies on tropospheric ozone over South and East Asia in 2030, Atmos. Chem. Phys., 14, 9259-9277, doi:10.5194/acp-14-9259-2014, 2014.

Chen, B., Xu, X., D, Yang, S., and Zhao, T. L.: Climatological perspectives of air transport from atmospheric boundary layer to tropopause layer over Asian monsoon regions during boreal summer inferred from Lagrangian approach, Atmos. Chem. Phys., 12, 5827–5839, doi:10.5194/acp-12-5827-2012. 2012.

Dentener F., Kinne S., Bond T., Boucher O., Cofala J., Generoso S., Ginoux P., Gong S., Hoelzemann J. J., Ito A., Marelli L., Penner J. E., Putaud J.-P., Textor C., Schulz M., Werf G. R. van der, and Wilson J.: Emissions of primary aerosol and precursor gases in the years 2000 and 1750 prescribed data-sets for AeroCom, Atmos. Chem. Phys., 6, 4321-4344, doi:10.5194/acp-6-4321-2006, 2006.

Druyan L. M., Fulakeza M. and Lonergan P.: The impact of vertical resolution on regional model simulation of the west African summer monsoon, Int. J. Climatol. 28: 1293–1314, DOI: 10.1002/joc.1636, 2008.

Edwards, J. M., and Slingo, A.: Studies with a flexible new radiation code .1. Choosing a configuration for a large-scale model, Quart. Jour. Roy. Met. Soc., 122(531), 689-719, doi:10.1002/qj.49712253107,1996.

Fadnavis, S., Semeniuk, K., Pozzoli, L., Schultz, M. G., Ghude, S. D., Das, S., and Kakatkar, R.: Transport of aerosols into the UTLS and their impact on the Asian monsoon region as seen in a global model simulation, Atmos. Chem. Phys., 13, 8771–8786, doi:10.5194/acp-13-8771-2013, 2013.

Fadnavis, S., Semeniuk, K., Schultz, M. G., Kiefer, M., Mahajan, A., Pozzoli, L., and Sonbawane, S.: Transport pathways of peroxyacetyl nitrate in the upper troposphere and lower stratosphere from different monsoon systems during the summer monsoon season. Atmos. Chem. and

Phys., 15, doi:10.5194/acp-15-11477-2015, 11477-11499, 2015.

Fadnavis, S., Semeniuk, K., Schultz, M. G., Mahajan, A., Pozzoli, L., Sonbawane, S., and Kiefer, M.: Transport pathways of peroxyacetyl nitrate in the upper troposphere and lower stratosphere from different monsoon systems during the summer monsoon season, Atmos. Chem. Phys. Discuss., 14, 20159–20195, doi:10.5194/acpd-14-20159-2014, 2014.

Fiore, A. M., Horowitz, L. W., Purves, D. W., Levy II, H., Evans, M. J., Wang, Y., Li, Q., and Yantosca, R. M.: Evaluating the contribution of changes in isoprene emissions to surface ozone trends over the eastern United States, J. Geophys. Res., 110, D12303, doi:10.1029/2004JD005485, 2005.

Flohn, H.: Large-scale aspects of the summer monsoon in South and East Asia, J. Meteor. Soc. Japan, 75, 180–186, doi: 551.553.21:551.589.5, 1957.

Flohn, H.: Recent investigations on the mechanism of the "Summer Monsoon" of Southern and Eastern Asia, Proc. Symp. Monsoon of the World, 1960.

Forster, F., Piers, M., and Keith, P. Shine: Radiative forcing and temperature trends from stratospheric ozone changes, J. Geophys Res, 102, 10841-10855, 1997.

Froidevaux, L., Livesey, N. J., Read, W. G., Jiang, Y. B., Jimenez, C. J., Filipiak, M. J., Schwartz, M. J., Santee, M. L., Pumphrey, H. C., Jiang, J. H., Wu, D. L., Manney, G. L., Drouin, B. J., Waters, J. W., Fetzer, E. J., Bernath, P. F., Boone, C. D., Walker, K. A., Jucks, K. W., Toon, G. C., Margitan, J. J., Sen, B., Webster, C. R., Christensen, L. E., Elkins, J. W., Atlas, E., Ueb, R. A., and Hendershot, R.: Early validation analyses of atmospheric profiles from EOS MLS on the Aura satellite. IEEE Trans. Geosci. Remote Sensing 44, 1106 − 1121, doi: 10.1109/TGRS.2006.864366, 2006.

Fu, R., Hu, Y. L., Wright, J. S., Jiang, J. H., Dickinson, R.E., Chen, M. X., Filipiak, M., Read, W. G., Waters, J. W.,and Wu, D. L.: Short circuit of water vapor and polluted air to the global stratosphere by convective transport over the Tibetan Plateau, P. Natl. Acad. Sci. USA, 103, 5664–5669, doi:10.1073/pnas.0601584103, 2006.

Ganzeveld, L. and Lelieveld, J.: Dry deposition parameterization in a chemistry general circulation model and its influence on the distribution of reactive trace gases, J. Geophys. Res., 100, 20999–21012, doi:10.1029/95JD02266, 1995.

Garny, H. and Randel, W. J.: Dynamic variability of the Asian monsoon anticyclone observed in potential vorticity and correlations with tracer distributions, J. Geophys. Res. Atmos., 118, 13,421–13,433, doi:10.1002/2013JD020908, 2013.

Gettelman, A., Kinnison, D. E., Dunkerton, T. J., and Brasseur, G. P.: Impact of monsoon circulations on the upper troposphere and lower stratosphere, J. Geophys. Res., 109, D22101, doi:10.1029/2004jd004878, 2004.

Ghude, S. D., Kulkarni, S. H., Jena, C., Pfister, G. G., Beig, G., Fadnavis, S., and van der A R. J.: Application of satellite observations for identifying regions of dominant sources of nitrogen oxides over the Indian Subcontinent, J. Geophys. Res., 118, 1–15, doi:10.1029/2012JD017811, 2013.

Goswami, B. N., Krishnamurthy, V., and Annamalai, H.: A broad-scale circulation index for the interannual variability of the Indian summer monsoon. Q. J. R. Meteorol. soc., 125, 611-633, doi: 10.1002/qj.49712555412, 1999.

Gu, D., Wang, Y., Smeltzer, C., and Boersma, K. F.: Anthropogenic emissions of NOx over China: Reconciling the difference of inverse modeling results using GOME-2 and OMI measurements, J. Geophys. Res. Atmos., 119, doi:10.1002/ 2014JD021644, 2014.

Hilboll, A., Richter, A., and Burrows, J. P.: Long-term changes of tropospheric NO2 over megacities derived from multiple satellite instruments, Atmos. Chem. Phys., 13, 4145–4169, doi:10.5194/acp-13-4145-2013, 2013.

Horowitz, L. W., Walters, S., Mauzerall, D. L., Emmons, L. K., Rasch, P. J., Granier, C., Tie, X., Lamarque, J., Schultz, M. G.,Tyndall, G. S., Orlando, J. J., and Brasseur, G. P.: A global simulation of tropospheric ozone and related tracers, Description and evaluation of MOZART, version 2, J. Geophys. Res., 108, 4784, doi:10.1029/2002JD002853, 2003.

Jacob, D. J., Logan, J. A., and Murti, P. P.: Effect of rising Asian emissions on surface ozone in the United States, Geophys. Res. Lett., 26, 2175–2178, doi:10.1029/1999GL900450, 1999.

Kärcher B. and U. Lohmann, A parameterization of cirrus cloud formation: Homogeneous freezing of supercooled aerosols, J. Geophy. Res. 107, NO. D2, 4010, 10.1029/2001JD000470, 2002.

Konopka, P., Grooß, J.U., Günther, G., Ploeger, F., Pommrich, R., Müller, R. and Livesey, N.: Annual cycle of ozone at and above the tropical tropopause: observations versus simulations with the Chemical Lagrangian Model of the Stratosphere (CLaMS), Atmos. Chem. Phys., 10(1), 121-132, doi: www.atmos-chem-phys.net/10/121/2010/, 2010.

Kunze, M., Braesicke, P., Langematz, U., Stiller, G., Bekki, S., Brühl, C., Chipperfield, M., Dameris, M., Garcia, R. and Giorgetta, M.: Influences of the Indian summer monsoon on water vapor and ozone concentrations in the UTLS as simulated by chemistry-climate models, J. Clim., 23(13), 3525-3544, doi: http://dx.doi.org/10.1175/2010JCLI3280.1, 2010.

Lacis Andrew, A., Donald Wuebbles, J., and Jennifer Logan A., Radiative Forcing of climate by Changes in the Vertical Distribution of Ozone, J. Geophys. Res., 95 , 9971-9981, doi: 10.1029/JD095iD07p09971, 1990.

Lawrence, M. G.: Atmospheric science: Asia under a high-level brown cloud, Nat. Geosci., 4, 352–353, doi:10.1038/ngeo1166, 2011.

Lei, W., Zhang, R., Tie, X., and Hess, P.: Chemical characterization of ozone formation in the Houston-Galveston area. J.Geophys.Res., 109, doi: 10.1029/2003JD004219, 2004.

Li, C. and Yanai M.: The onset and interannual variability of the Asian summer monsoon in relation to land–sea thermal contrast, J. Clim. 9: 358–375, doi: http://dx.doi.org/10.1175/1520-0442(1996)009<0358:TOAIVO>2.0.CO;2, 1996.

Li, Q., Jiang, J. H., Wu, D. L., Read, W. G., Livesey, N. J., Waters, J. W., Zhang, Y., Wang, B.,. Filipiak, M. J, Davis, C. P., Turquety, S., Wu, S., Park, R. J., Yantosca, R. M., and Jacob, D. J.: Convective outflow of south Asian pollution: a global CTM simulation compared with EOS MLS observations, Geophys. Res. Lett., 32, doi: http://dx.doi.org/10.1029/2005GL022762, doi: 10.1029/2005GL022762, 2005.

Livesey, N. J., Read, W. G., Filipiak, M. J., Froidevaux, L., Harwood, R. S., Jiang, J. H., Jimenez, C., Pickett, H. M., Pumphrey, H. C., Santee, M. L., Schwartz, M. J., Waters, J. W., and Wu, D. L.: EOS MLS Version 1.5 Level 2 data quality and description document, JPL, California, 2005.

Livesey, N. J., Read, W. G., Froideveaux, L., Lambert, A., Manney, G. L., Pumphrey, H. C., Santee, M. L., Schwartz, M. J., Wang, S., Cofield, R. E., Cuddy, D. T., Fuller, R. A., Jarnot, R. F., Jiang, J. H., Knosp, B. W., Stek, P. C., Wagner, P. A., and Wu, D. L.: Version 3.3 Level 2 data quality and description document. Tech Rep. JPL D-33509, Jet Propulsion Laboratory, available at: http://mls.jpl.nasa.gov (last access: 17 August 2015), 2011.

Lohmann, U., J. Feichter, C. C. Chuang, and J. E. Penner, Predicting the number of cloud droplets in the ECHAM GCM, J. Geophys. Res., 104, 9169 – 9198, 1999.

Meehl, G. A.: Coupled land-ocean-atmosphere processes and South Asian monsoon variability, Science, 266, 263–267, doi: 10.1126/science.266.5183.263, 1994.

Myhre, G., et al., Anthropogenic and natural radiative forcing, in Climate Change 2013: The Physical Science Basis. Contribution of Working Group I to the Fifth Assessment Report of the Intergovernmental Panel on Climate Change, edited by T. F. Stocker et al., pp. 659–740, Cambridge Univ. Press, Cambridge, U. K., and New York, 2013.

Park, M., Randel, W. J., Emmons, L. K., Bernath, P. F., Walker, K. A., and Boone, C. D.: Chemical

19

isolation in the Asian monsoon anticyclone observed in Atmospheric Chemistry Experiment (ACE-FTS) data, Atmos. Chem. Phys., 8, 3, 757-764, doi: www.atmos-chem-phys.net/8/757/2008/, 2008.

Park, M., Randel, W. J., Emmons, L. K., and Livesey, N. J.:Transport pathways of carbon monoxide in the Asian summer monsoon diagnosed from Model of Ozone and Related Tracers (MOZART), J. Geophys. Res., 114, D08303, doi:10.1029/2008jd010621, 2009.

Park, M., Randel, W. J., Gettelman, A., Massie, S. T., and Jiang, J.H.: Transport above the Asian summer monsoon anticyclone inferred from Aura Microwave Limb Sounder tracers, J. Geophys.Res., 112, D16309,doi:10.1029/2006jd008294, 2007.

Park, M., Randel, W. J., Kinnison, D. E., Garcia, R. R., and Choi, W.: Seasonal variation of methane, water vapour, and nitrogen oxides near the tropopause: Satellite observations and model simulations, J. Geophys. Res., 109, D03302, doi:10.1029/2003JD003706, 2004.

Penki, R. K. and Kamra, A. K.: Lightning distribution with respect to the monsoon trough position during the Indian summer monsoon season, J. Geophy. Res., 118, 4780–4787, doi:10.1002/jgrd.50382, 2013.

Ploeger, F., Gottschling, C., Griessbach, S., Grooß, J.-U., Guenther, G., Konopka, P., Müller, R., Riese, M., Stroh, F., Tao, M., Ungermann, J., Vogel, B., and von Hobe, M.: A potential vorticity-based determination of the transport barrier in the Asian summer monsoon anticyclone, Atmos. Chem. Phys., 15, 13145-13159, doi:10.5194/acp-15-13145-2015, 2015.

Pozzoli, L., Bey, I., Rast, J. S., Schultz, M. G., Stier, P., and Feichter, J.: Trace gas and aerosol interactions in the fully coupled model of aerosol-chemistry-climate ECHAM5- HAMMOZ: 1. Model description and insights from the spring 2001 TRACE-P experiment, J. Geophys. Res., 113, D07308, doi:10.1029/2007JD009007, 2008a.

Pozzoli, L., Bey, I., Rast, J. S., Schultz, M. G., Stier, P., and Feichter, J.: Trace gas and aerosol interactions in the fully coupled model of aerosol-chemistry-climate ECHAM5- HAMMOZ: 2. Impact of heterogeneous chemistry on the global aerosol distributions, J. Geophys. Res., 113, D07309, doi:10.1029/2007JD009008, 2008b.

Pozzoli, L., Janssens-Maenhout, G., Diehl, T., Bey, I., Schultz, M. G., Feichter, J., Vignati, E., and Dentener, F.: Re-analysis of tropospheric sulfate aerosol and ozone for the period 1980–2005 using the aerosol-chemistry-climate model ECHAM5-HAMMOZ, Atmos. Chem. Phys., 11, 9563–9594, doi:10.5194/acp-11-9563-2011, 2011.

Rajeevan M., Bhate J.,. Kale J.D and Lal B.:Development of High Resolution Daily Gridded Rainfall Data for the Indian Region, Met. Monograph Climatology No. 22/2005, National Climate Centre India Meteorological Department. Pune 411 005, India, 2005.

Rajagopalan, B., and Molnar, P.: Signatures of Tibetan Plateau heating on Indian summer monsoon rainfall variability, J. Geophys. Res. Atmos., 118, 1170–1178, doi:10.1002/jgrd.50124, 2013.

Ranalkar, M. R. and Chaudhari, H. S.: Seasonal variation of lightning activity over the Indian subcontinent, Meteorol. Atmos.Phys., 104, 125–134, doi: 10.1007/s00703-009-0026-7, 2009.

Randel, W. J., and Park M.: Deep convective influence on the Asian summer monsoon anticyclone and associated tracer variability observed with Atmospheric Infrared Sounder (AIRS), J. Geophys. Res.,111, D12314, doi:10.1029/2005JD006490, 2006.

Randel, W. J., Park, M., Emmons, L., Kinnison, D., Bernath, P., Kaley Walker, A., Boone, C., and Pumphrey, H.: Asian Monsoon Transport of Pollution to the Stratosphere Science, 328(5978), 611-613, doi: 10.1126/science.1182274, 2010.

Randel, W. J., Wu, F., Gettelman, A., Russell, J. M., Jawodny, J. M., and Oltmans, S. J.: Seasonal variation of water vapor in the lower stratosphere observed in Halogen Occultation Experiment data, J. Geo-phys. Res., 106, 14,313 – 14,325, doi: 0148-0227/01/2001JD900048509.00, 2001.

Rap, A., Richards, N., A., D., Forster, P., M., Monks, S., Arnold, S., R., Chipperfield, M.: Satellite

constraint on the tropospheric ozone radiative effect, Geophys. Res. Lett, 42, 5<u>074-5081</u>.doi:10.1002/2015GL064037, 2015.

Revell, L. E., Tummon, F., Stenke, A., Sukhodolov, T., Coulon, A., Rozanov, E., Garny, H., Grewe, V., and Peter, T.: Drivers of the tropospheric ozone budget throughout the 21st century under the medium-high climate scenario RCP 6.0, Atmos. Chem. Phys., 15, 5887-5902, doi:10.5194/acp-15-5887-2015, 2015.

Richter, A., John Burrows, P., Hendrik, N., Granier C., and Niemeier, U.: Increase in tropospheric nitrogen dioxide over China observed from space; 437, doi:10.1038/nature04092, 2005.

Riese, M., Ploeger, F., Rap, A., Vogel, B., Konopka, P., Dameris, M. and Forster, P.: Impact of uncertainties in atmospheric mixing on simulated UTLS composition and related radiative effects, J. Geophys. Res.: Atmos., 117(D16), doi: 10.1029/2012JD017751, 2012.

Rodwell, M. J. and Hoskins, B. J.: Monsoons and the dynamics of deserts, QJRMS, 122(534), 1385-1404, doi: 10.1002/qj.49712253408, 1995.

Roeckner, E., Bauml, G., Bonaventura, L., Brokopf, R., Esch, M., Giorgetta, M., Hagemann, S., Kirchner, I., Kornblueh, L., Manzini, E., Rhodin, A., Schlese, U., Schulzweida, U., and Tompkins, A.: The atmospehric general circulation model ECHAM5: Part 1, Tech. Rep. 349, Max Planck Institute for Meteorology,Hamburg, 2003.

Sander, S. P., Fried, R. R., Barker, J. R., Golden, D. M., Kurylo, M. J.,Wine, P. H., J. Abbatt, P. D., 25 Burkholder, J. B., Kolb, C. E., Moortgat, G. K., Huie, R. E., and Orkin, V. L.: Chemical kinetics and photochemical data for use in atmospheric studies, evaluation number 14, JPL Publ. 02-25, Jet Propul. Lab., Calif. Inst. Of Technol., Pasadena, available at: http://jpldataeval.jpl.nasa.gov/pdf/JPL_02-25_rev02.pdf, 2003.

Schneider, P. and van der A. R. J.: A global single-sensor analysis of 2002–2011 tropospheric nitrogen dioxide trends observed from space, J., Geophy. Res., 117, D16309, doi:10.1029/2012JD017571, 2012.

Schoeberl, M. R., Duncan, B. N., Douglass, A. R., Waters, J., Livesey, N., Read, W., and Filipiak, M.: The carbon monoxide tape recorder. Geophys. Res. Lett., 33(12), doi: 10.1029/2006GL026178, 2006.

Schultz, M. G., Heil, A., Hoelzemann, J. J., Spessa, A., Thonicke, K., Goldammer, J. G., Held, A. C., Pereira, J. M. C., and van het Bolscher, M.: Global wildland fire emissions from 1960 to 2000, Global Biogeochem. Cy., 22, GB2002, doi:10.1029/2007GB003031, 2008.

Schultz, M., Backman, L., Balkanski, Y., Bjoerndalsaeter, S., Brand, R., Burrows, J., Dalsoeren, S., de Vasconcelos, M., Grodtmann, B., Hauglustaine, D., Heil, A., Hoelzemann, J., Isaksen, I., Kaurola, J., Knorr, W., Ladstaetter-Weienmayer, A., Mota, B., Oom, D., Pacyna, J., Panasiuk, D., Pereira, J., Pulles, T., Pyle, J., Rast, S., Richter, A., Savage, N., Schnadt, C., Schulz, M., Spessa, A., Staehelin, J., Sundet, J., Szopa, S., Thonicke, K., van het Bolscher, M., van Noije, T., van Velthoven, P., Vik, A. and Wittrock, F.: REanalysis of the TROpospheric chemical composition over the past 40 years (RETRO). A long-term global modeling study of tropospheric chemistry. Final Report, Tech. rep., Max Planck Institute for Meteorology, Hamburg, Germany, 2007.

Schultz, M.G., Heil A., Hoelzemann, J. J., Spessa, A., Thonicke, K., Goldammer, J.,. Held, A.C, Pereira, J. M., Van Het Bolscher, M.: Global Wildland Fire Emissions from 1960 to 2000, doi:10.1029/2007GB003031 , Global Biogeochemical Cycles 22 (GB2002) : 17 PP, 2005

Sillman, S.: The use of NOy, H_2O_2, and HNO_3 as indicators for ozone-NO_x-hydrocarbon sensitivity in urban locations. J. Geophys. Res., 100, 14,175–14,188, doi: 10.1029/94JD02953, 1995.

Sinha, V., Kumar, V., and Sarkar, C.: Chemical composition of pre-monsoon air in the Indo-Gangetic Plain measured using a new air quality facility and PTR-MS: high surface ozone and strong influence of biomass burning, Atmos. Chem. Phys., 14, 5921–5941, 2014. doi:10.5194/acp-14-

5921-2014, 2014.

Søvde, O. A., Hoyle, C. R., Myhre, G., and Isaksen, I. S. A.: The HNO3 forming branch of the HO2 + NO reaction: pre-industrial-to-present trends in atmospheric species and radiative forcings, Atmos. Chem. Phys., 11, 8929–8943, 2011; doi:10.5194/acp-11-8929-2011, 2011.

Stevenson, D. S., P. J. Young, Vaishali, N., Lamarque, J. F., Drew, T., Shindell, Voulgarakis, A., and Skeie R. B.: Tropospheric ozone changes, radiative forcing and attribution to emissions in the Atmospheric Chemistry and Climate Model Intercomparison Project (ACCMIP), Atmos. Chem. Phys., 13, 3063-3085, doi:10.5194/acp-13-3063-2013, 2013.

Stier, P., Feichter, J., Kinne, S., Kloster, S., Vignati, E., Wilson, J., Ganzeveld, L., Tegen, I., Werner, M., Balkanski, Y., Schulz, M., Boucher, O., Minikin, A., and Petzold, A.: The aerosol-climate model ECHAM5-HAM, Atmos. Chem. Phys., 5, 1125–1156, doi:10.5194/acp-5-1125-2005, 2005.

Thuburn, J. and Craig, G.C.: On the temperature structure of the tropical substratosphere, Journal of Geophysical Research: Atmospheres, 107(D2), doi: 10.1029/2001JD000448, 2002.

Tie, X. X., Zhang, R., Brasseur, G., Emmons, L., and Lei, W.:Effects of lightning on reactive nitrogen and nitrogen reservoir species in the troposphere, J. Geophys. Res.-Atmos., 106, 3167– 3178, doi:10.1029/2000JD900565, 2001.

Tie, X., Madronich, S., Li, G.H., Ying, Z.M., Zhang, R., Garcia, A., Lee-Taylor, and J., Y. Liu. Characterizations of chemical oxidants in Mexico City: a regional chemical/dynamical model (WRF-Chem) study, Atmos. Environ., 41, 1989–2008, doi:10.1016/j.atmosenv.2006.10.053, 2007.

Tiedtke, M.: A comprehensive mass flux scheme for cumulus parameterization in large-scale models, Mon. Weather Rev., 117(8), 1779–1800, 1989.

Tobo, Y., Iwasaka, Y., Zhang, D., Shi, G., Kim, Y. S., Tamura, K., and Ohashi, T.: Summertime ''ozone valley'' over the Tibetan Plateau derived from ozonesondes and EP/TOMS data, Geophys. Res. Lett., 35, L16801, doi:10.1029/2008GL03434, 2008.

Vernier, J.-P., T. D. Fairlie, M. Natarajan, F. G. Wienhold, J. Bian, B. G. Martinsson, S. Crumeyrolle, L. W. Thomason, and Bedka, K.: Increase in upper tropospheric and lower stratospheric aerosol levels and its potential connection with Asian Pollution, J. Geophys. Res. Atmos., 120, 1608–1619, doi:10.1002/2014JD022372, 2015.

Vinoj, V., Rasch, P.J., Wang, H., Yoon, J.H., Ma, P.L., Landu, K. and Singh, B.: Short-term modulation of Indian summer monsoon rainfall by West Asian dust, Nature Geoscience, 7(4), 308-313, doi:10.1038/ngeo2107, 2014.

Vogel B., Günther G., Müller R., Grooß, and Riese M.: Impact of different Asian source regions on the composition of the Asian J.-u. monsoon anticyclone and of the extratropical lowermost stratosphere, Atmos. Chem. Phys., 15, 13699–13716, doi:10.5194/acp-15-13699-2015, 2015.

Vogel, B., Günther, G., Müller, R., Grooß, J.-U., Afchine, A., Bozem, H., Hoor, P., Krämer, M., Müller, S., Riese, M., Rolf, C., Spelten, N., Stiller, G. P., Ungermann, J., and Zahn, A.: Long-range transport pathways of tropospheric source gases originating in Asia into the northern lower stratosphere during the Asian monsoon season 2012, Atmos. Chem. Phys. Discuss., doi:10.5194/acp-2016-463, revised paper accepted for ACPD, 2016.

Waters, J. W., Froidevaux, L., Harwood, R.S., Jarnot, R.F., Pickett, H. M., Read, W. G., Siegel, P. H., Cofield, R. E., Filipiak, M. J., Flower, D. A., Holden, J. R., Lau, G. K., Livesey, N. J., Manney, G. L., Pumphrey, H. C., Santee, M. L., Wu, D. L., Cuddy, D. T., Lay, R. R., Loo, M. S., Perun, V. S., Schwartz, M. J., Stek, P. C., Thurstans, R. P., Boyles, M. A., Chandra, S., Chavez, M. C., Chen, G. S., Chudasama, B. V., Dodge, R., Fuller, R. A., Girard, M.A., Jiang, J. H., Jiang, Y., Knosp, B. W., LaBelle, R. C., Lee, K. A., Miller, D., Oswald, J. E., Patel, N. C., Pukala, D. M., Quintero, O., Scaff, D. M., Snyder, W. V., Tope, M. C., Wagner, P. A., and Walch, M. J.:

The Earth Observing System Microwave LimbSounder (EOS MLS) on the Aura satellite. IEEE Trans, Geosci., Remote Sensing, 44, 1075 – 1092, doi: 10.1109/TGRS.2006.873771, 2006.

Wild, O., and Akimoto, H.: Intercontinental transport of ozone and its precursors in a three-dimensional global CTM, J., Geophys. Res., 106(D21), 27729-27744, doi: http://dx.doi.org/10.1029/2000JD000123, 2001.

Wu, G. X., and Zhang, Y. S.: Tibetan Plateau forcing and the timing of the monsoon onset over South Asia and the South China Sea, Mon Wea Rev 126:913–927, doi: http://dx.doi.org/10.1175/1520-0493(1998)126<0913:TPFATT>2.0.CO;2, 1998.

Xiong, X., Houweling S., Wei J., Maddy E., Sun F., and Barnet C.: Methane plume over south Asia during the monsoon season: satellite observation and model simulation, Atmos. Chem. Phys., 9, 783–794, doi:10.5194/acp-9-783-2009, 2009.

Yamaji, K., T. Ohara, I. Uno, H. Tanimoto, J. Kurokawa, and Akimoto H.: Analysis of the seasonal variation of ozone in the boundary layer in East Asia using the Community Multiscale Air Quality model: what controls surface ozone levels over Japan?, Atmos. Environ., 40, 1856–1868, 2006.

Yanai, M., Li, C., Song, Z.: Seasonal heating of the Tibetan Plateau and its effects on the evolution of the Asian summer monsoon, J Meteor Soc Japan, 70, 189–221, 1992.

Zhang, R.W., Lei, X., and Hess, T. P.: Industrial emissions cause extreme diurnal urban ozone variability. Proc. Natl. Acad. Sci., 101, 6346–6350, doi: 10.1073/pnas.0401484101, 2004.

Zhao, B., Wang, S. X., Liu, H., Xu, J. Y., Fu, K., Klimont, Z., Hao, J. M., He, K. B., Cofala, J., and Amann, M.: NOx emissions in China: historical trends and future perspectives, Atmos. Chem. Phys., 13, 9869–9897, doi:10.5194/acp-13-9869-2013, 2013.
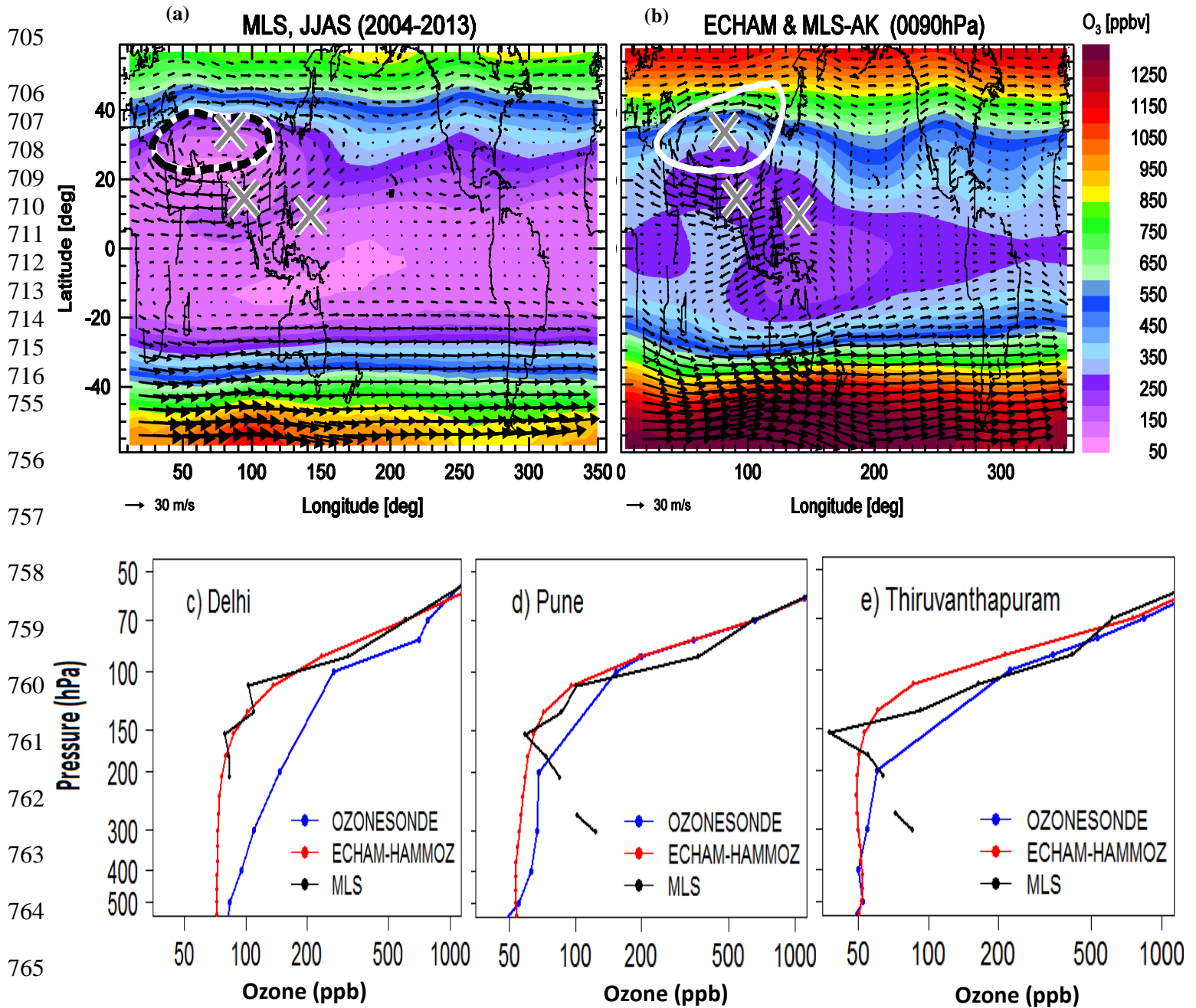
Figure 1: Distribution of ozone mixing ratio (ppb) during the monsoon season (June-September) obtained from (a) MLS observations at 100 hPa, and (b) from ECHAM-HAMMOZ at 90hPa. Black arrows indicate wind vectors, the black dashed contour shows the PV-gradient based transport barrier of the anticyclone (calculated following Ploeger et al., 2015), and the white contour shows the 270m geopotential height anomaly, corresponding to the anticyclone edge definition by Barret et al. (2016) Meteorological data shows climatological July fields from ERA-Interim reanalysis (a) ERA-Interim

773 reanalysis and (b) ECHAM5-HAMMOZ. The ECHAM5-HAMMOZ ozone distribution is smoothed

774 using the MLS averaging kernel. Grey crosses highlight the regions of the Tibetan plateau, Bay of

775 Bengal and South China Sea. Bottom panels show the vertical distribution of seasonal (June-

776 September) mean ozone mixing ratios (ppb) from ozonesonde (2001-2009), MLS (2004-2013) and

777 ECHAM5-HAMMOZ CTRL simulation at the (c) Delhi, (d) Pune, and (e) Thiruvananthpuram Indian

778 stations.

779
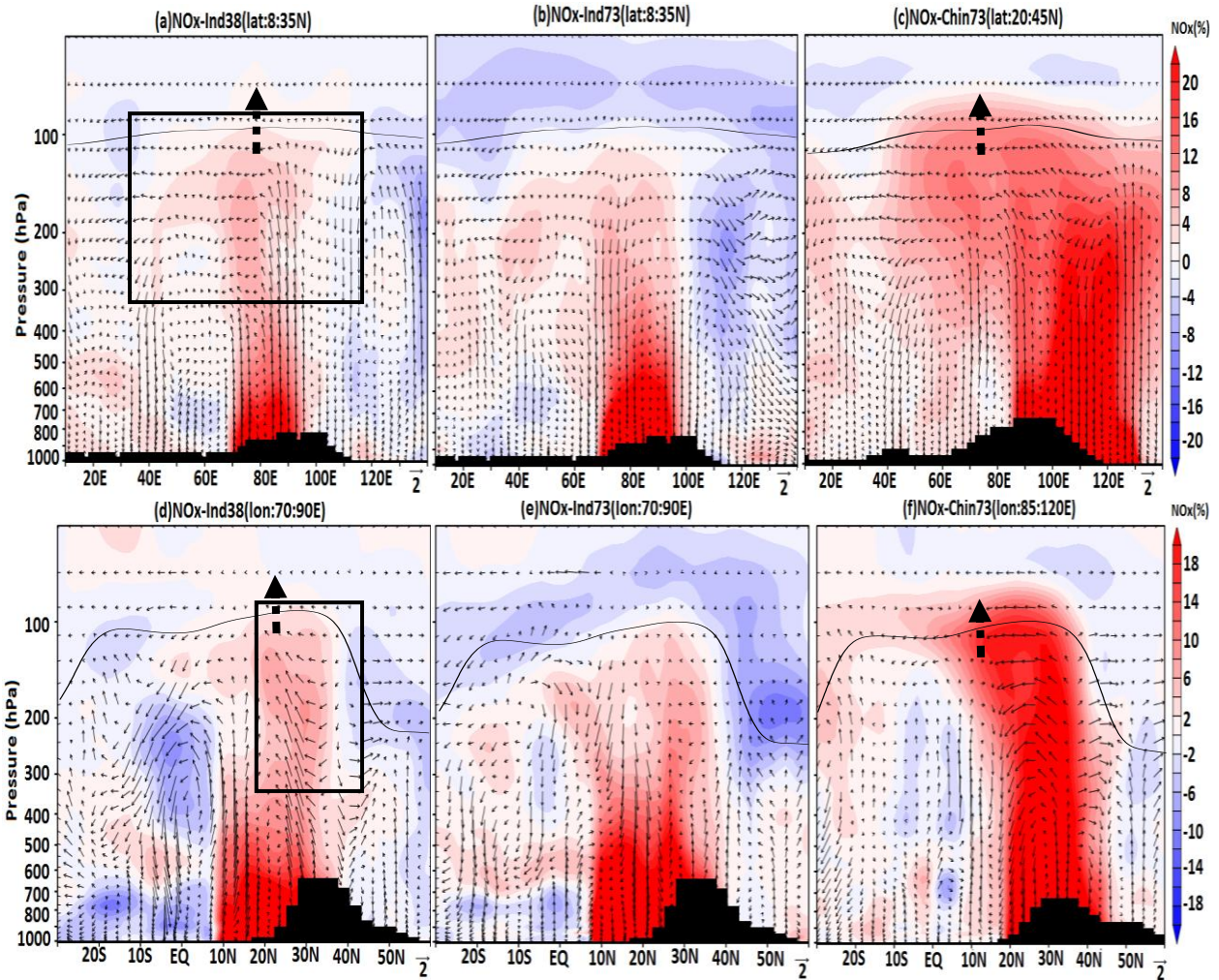
Figure 2: Longitude pressure cross-sections of percentage NO$_x$ anomalies averaged for the monsoon season (June-September) obtained from (a) Ind38 (averaged over 8ºN-35ºN), (b) Ind73 (averaged over 8ºN-35ºN), and (c) Chin73 (averaged over 20ºN-45ºN) simulations. Latitude pressure cross-sections of percentage NO$_x$ anomalies averaged for the monsoon season (June-September) obtained from (d) Ind38 (averaged over 70ºE-90ºE), (e) Ind73 (averaged over 70ºE-90ºE), and (f) Chin73 (averaged over 85ºE-120ºE) simulations. Black arrows indicate wind vectors (the vertical velocity field has been scaled by 300), the black line represents the tropopause, and the black dashed arrows indicate the cross tropopause transport. The black boxes show the outline of the anticyclone.
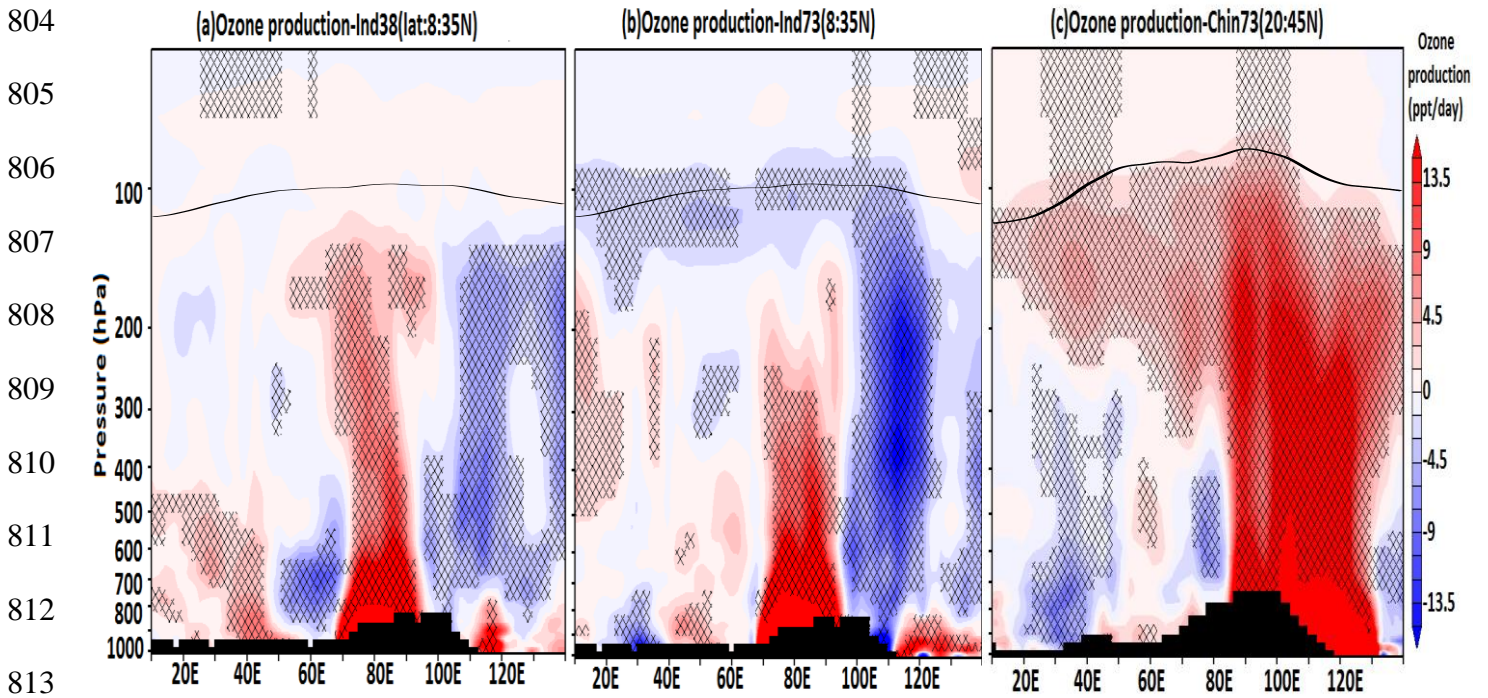
Figure 3: Longitude pressure cross-section of changes in net ozone production (ppt/day) due to enhanced NO$_x$ with respect to the CTRL simulation, averaged for the monsoon season (June-September) obtained from (a) Ind38 (averaged over 8ºN-35ºN), (b) Ind73 (averaged over 8ºN-35ºN), and (c) Chin73 (over 20ºN-45ºN) simulations. The black line shows the tropopause while black hatched lines indicate 95% confidence level.
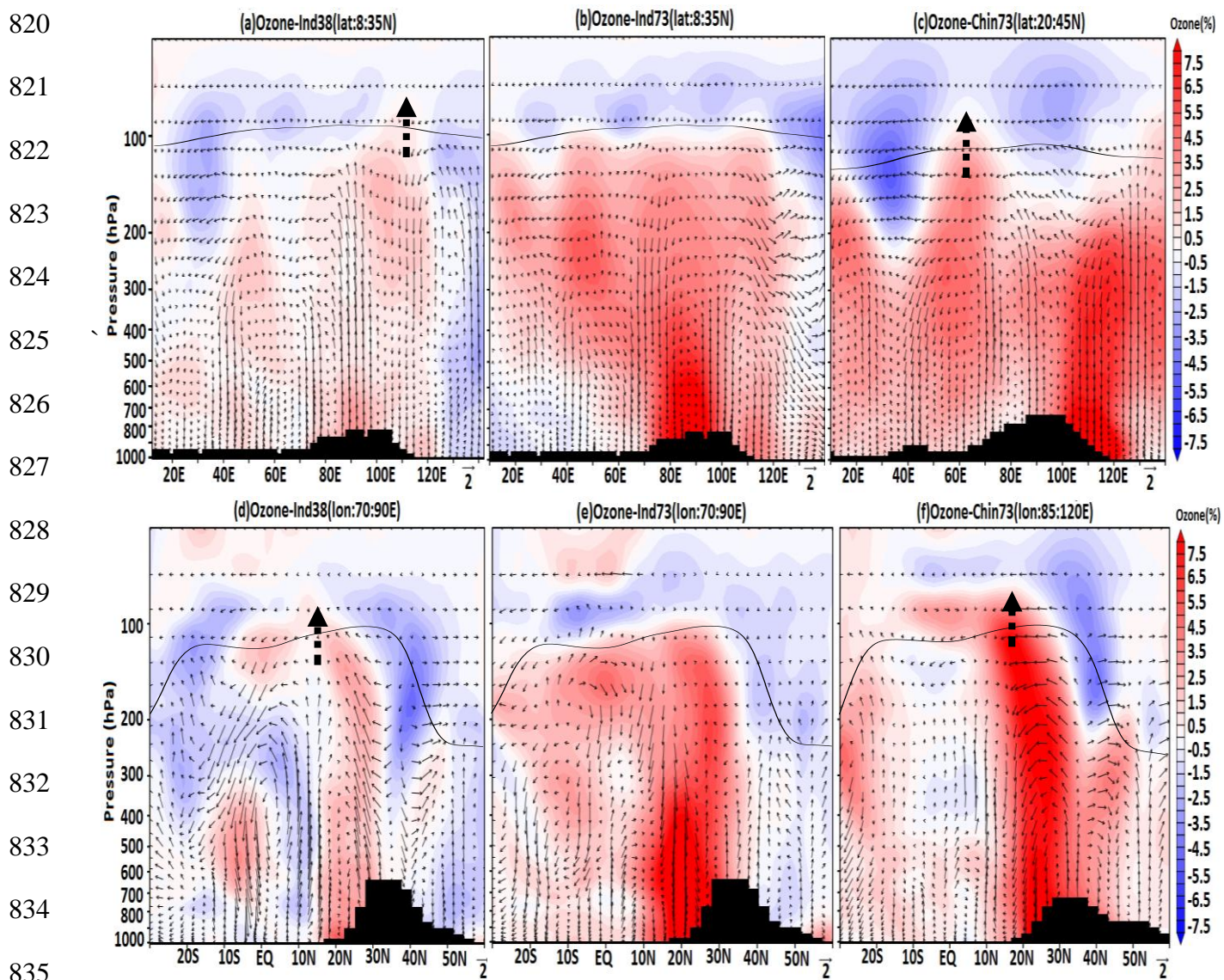
Figure 4: Longitude pressure cross-section of percentage ozone anomalies averaged for the monsoon season (June-September) obtained from (a) Ind38 (averaged over 8ºN-35ºN), (b) Ind73 (averaged over 8ºN-35ºN), and (c) Chin73 (averaged over 20ºN-45ºN) simulations. Latitude pressure cross-section of percentage ozone anomalies averaged for the monsoon season (June-September) obtained from (d) Ind38 (averaged over 70ºE-90ºE), (e) Ind73 (averaged over 70ºE-90ºE), and (f) Chin73 (averaged over 85ºE-120ºE) simulations. Black arrows indicate wind vectors. The vertical velocity field has been scaled by 300. The black line represents the tropopause, and the black dashed arrows indicate the cross tropopause transport.

28

Figure 5: Latitude-longitude cross-section of percentage NO$_x$ anomalies averaged for the monsoon season (June-September) at 110 hPa obtained from (a) Ind38, (b) Ind73, and (c) Chin73 simulations. Panels (d-f) show the same but for percentage ozone anomalies at 110 hPa for the (d) Ind38, (e) Ind73, and (f) Chin73 simulations. Black arrows indicate horizontal winds at 110 hPa. The red box in panel (a) indicates the ASM anticyclone region used to compute the associated radiative forcing regional average.

861

862

863

864

865

866

867

868

869

870   Figure 6: Latitude-longitude distribution of changes in ozone radiative forcing (in mW m^{-2}) for the (a)

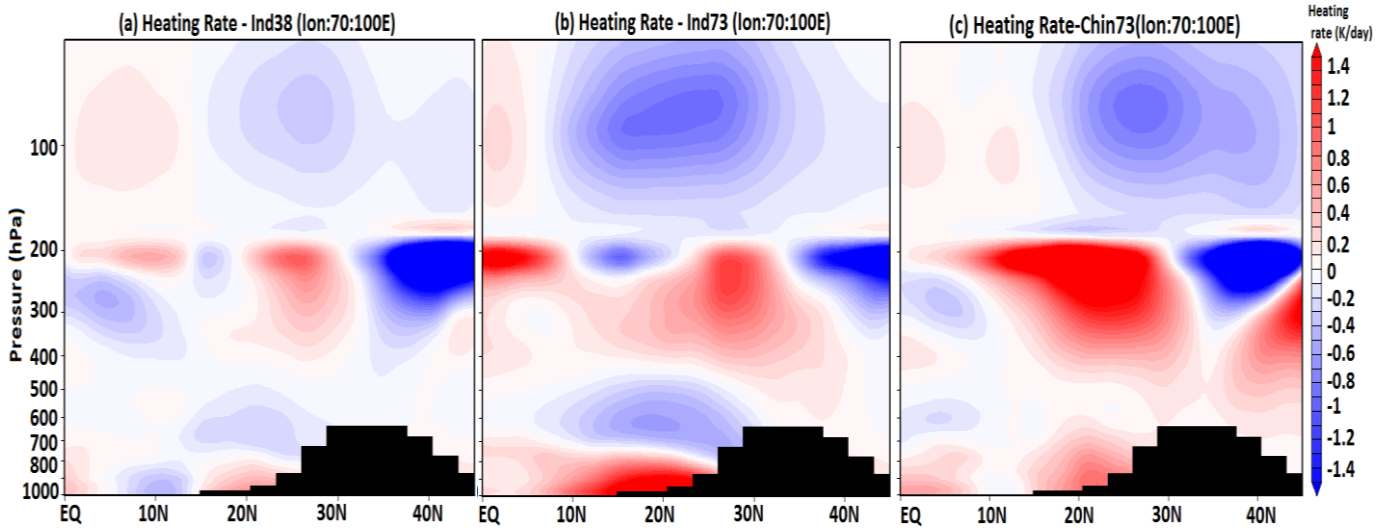871   Ind38, (b) Ind73, and (c) Chin73 perturbed simulations, compared to the CTRL simulation.

872
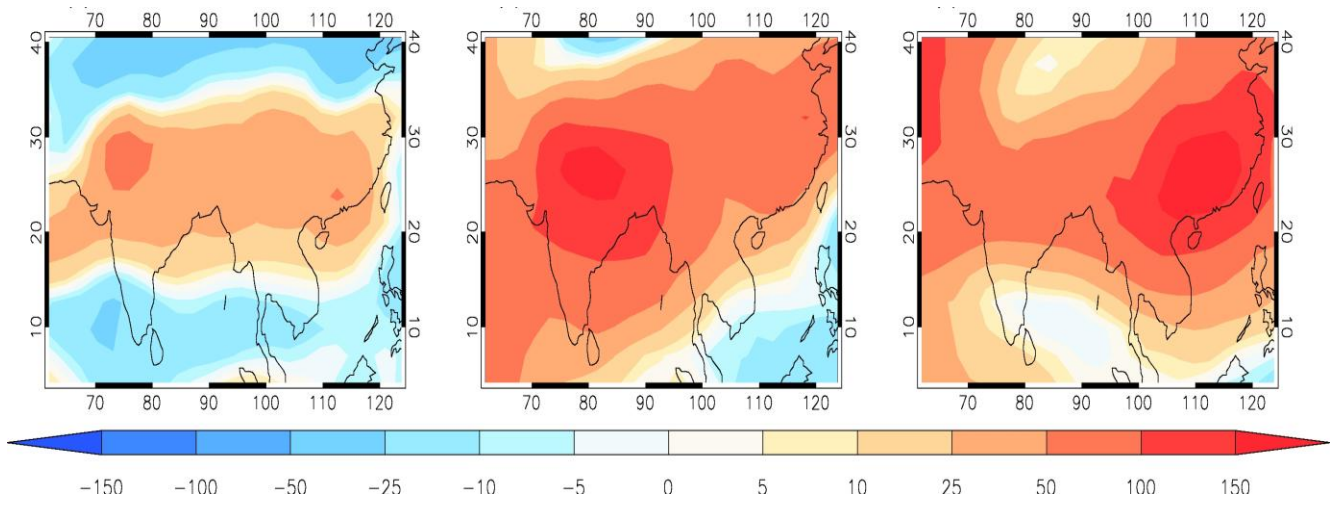
873

Figure 7: Latitude- pressure distribution of ozone heating rate changes (in K/day) for the (a) Ind38 (averaged over 70º-100ºE), (b) Ind73 (averaged 70º-100ºE), and (c) Chin73 (averaged over 70º -100º E) perturbed simulations, compared to the CTRL simulation.
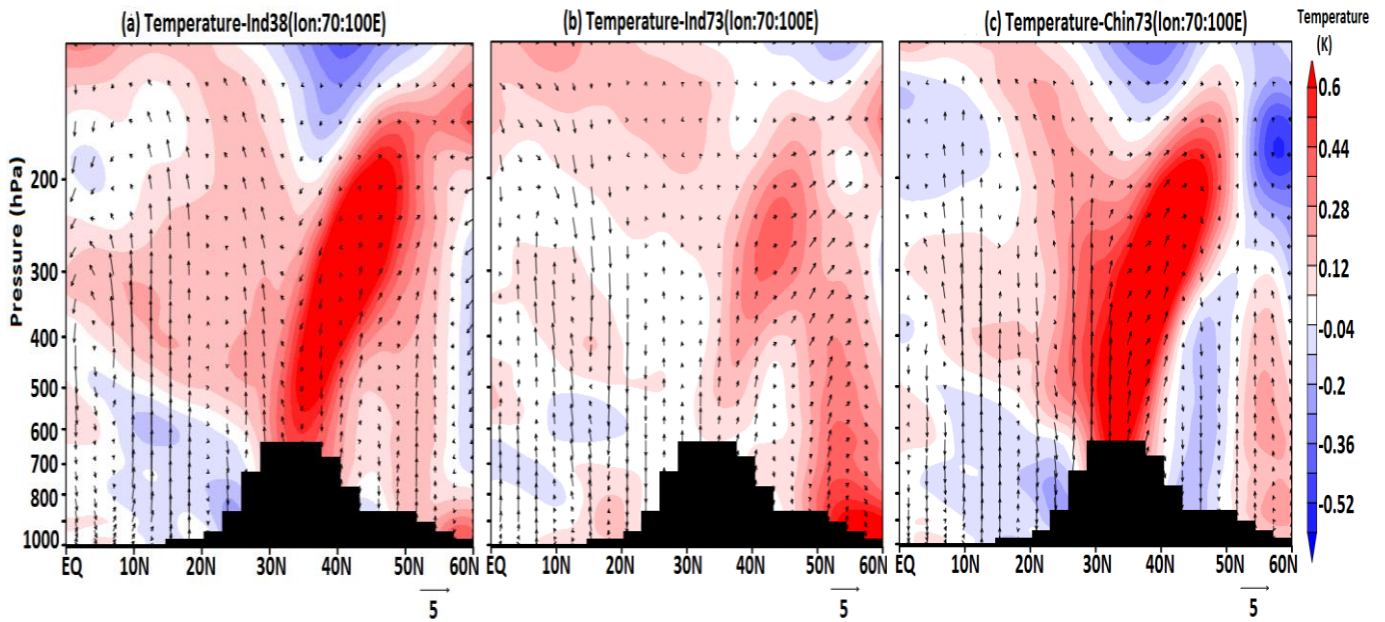
886

887

888

Figure 8: Latitude pressure cross-section of temperature anomalies (K) averaged for the monsoon season (June-September) and over 70ºE-100ºE obtained from (a) Ind38-CTRL, (b) Ind73-CTRL, and (c) Chin73-CTRL simulations. Black arrows indicate wind vectors (the vertical velocity field has been scaled by 300).

901

902

903

904

905

906

907

908

909

910
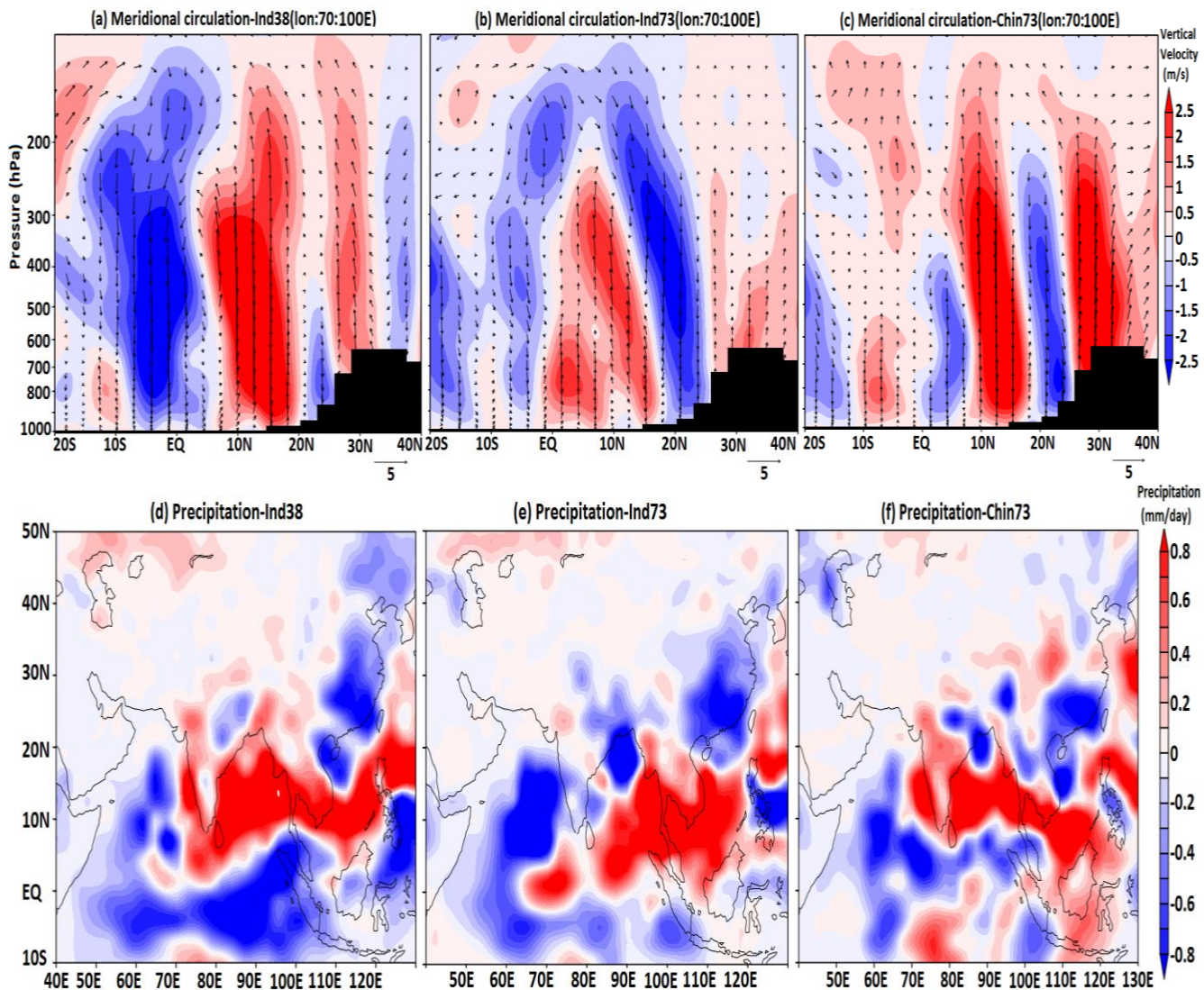

Figure 9: Difference in the meridional circulation due to enhanced NO$_X$ emissions averaged for the monsoon season (June-September) and over 70ºE-100ºE for (a) Ind38-CTRL (b) Ind73-CTRL (c) Chin73-CTRL simulations. Shaded contours indicate the anomalies in vertical velocity (m/s). The vertical velocity field has been scaled by 300. Precipitation anomalies (mm/day) averaged for the monsoon season (June-September) obtained from (d) India38-CTRL (e) Ind73-CTRL, and (f) Chin73-CRTL simulations.